MmWave V2V Localization in MU-MIMO Hybrid Beamforming

Jaswinder Lota, *Senior Member, IEEE*, Shihao Ju, Student Member, IEEE, Ojas Kanhere, Student Member, IEEE, Theodore S. Rappaport, *Fellow, IEEE* and Andreas Demosthenous, *Fellow, IEEE*

Abstract - Recent trends for vehicular localization in millimetre-wave (mmWave) channels include employing a combination of parameters such as angle of arrival (AOA), angle of departure (AOD), and time of arrival (TOA) of the transmitted/received signals. These parameters are challenging to estimate, which along with the scattering and random nature of mmWave channels, and vehicle mobility lead to errors in localization. To circumvent these challenges, this paper proposes mmWave vehicular localization employing difference of arrival for time and frequency, with multiuser (MU) multiple-input-multiple-output (MIMO) hybrid beamforming; rather than relying on AOD/AOA/TOA estimates. The vehicular localization can exploit the number of vehicles present, as an increase in the number of vehicles reduces the Cramér-Rao bound (CRB) of error estimation. At 10 dB signal-to-noise ratio (SNR) both spatial multiplexing and beamforming result in comparable localization errors. At lower SNR values, spatial multiplexing leads to larger errors compared to beamforming due to formation of spurious peaks in the cross ambiguity function. Accuracy of the estimated parameters is improved by employing an extended Kalman filter leading to a root mean square (RMS) localization error of approximately 6.3 meters.

***Index Terms*— Hybrid beamforming, localization, mmWave, MU-MIMO, V2V.**

I. Introduction

Next generation vehicles are required to be fully connected and communicate with each other and the transport infrastructure. These connections will increase safety and deliver intelligent services, with a vision of fully autonomous vehicles in the future. Vehicles will require cellular networks with high throughput speeds to share their location, speed, and other sensor information with low latency. The Third Generation Partnership Project (3GPP) release 16 shows the fifth-generation (5G) network operating between 0.5 GHz-100 GHz would facilitate such data transfer for transportation from vehicle-to-vehicle (V2V) [1], [2]. Millimetre-wave (mmWave) frequencies can support high peak data rates of several gigabits per second required for various automated functions such as localization [3].

Current mmWave localization techniques are applicable to static channels, and the transmitter (Tx)-receiver (Rx) mobility is not quantified. Most techniques require robust beam switching/control strategies for accurate estimation of the angle of departure (AOD)/angle of arrival (AOA). Beam-tracking becomes challenging due to more vehicles requiring robust, fast beam switching techniques. Joint time difference of arrival (TDOA)/frequency difference of arrival (FDOA) estimation under these conditions are potential candidates for localization estimates.

This paper aims to apply the joint TDOA/FDOA approach with multiuser (MU) multiple-input multiple output (MIMO) hybrid beamforming (HB) for vehicle localization at mmWave frequencies. The Fisher information matrix (FIM) is used to access the data quality among multiple vehicles to manage the mmWave channel and optimize the emitter vehicle location subject to communication constraints. Channel sounding is assumed for HB to determine the channel state information (CSI), and joint spatial division multiplexing is employed to determine the precoding and coding weights for the selected system configuration.

The main contributions in this paper are enumerated:

- We derive a closed-form expression of Cramér-Rao Bound (CRB) of the parameter estimation and analyze the accuracy of cross ambiguity function (CAF) for TDOA/FDOA localization in beamforming (BF) and spatial multiplexing (SM) modes. CRB estimation indicates that increasing the number of vehicles reduces the estimation error. Therefore, localization with TDOA/FDOA estimation can accordingly exploit the number of vehicles present in V2V channels. Results show that higher accuracy is achieved in BF than in SM.
- We propose a TDOA/FDOA estimation approach

J. Lota is with the Department of Engineering and Computing, University East London, London E16 2RD UK (e-mail: j.lota@uel.ac.uk). S. Ju, O. Kanhere and T. S. Rappaport are with NYU WIRELESS and Tandon School of Engineering, New York University, Brooklyn, NY 11201 USA (e-mail: shao@nyu.edu; ojask@nyu.edu; tsr@nyu.edu).

A. Demosthenous is with the Department of Electronic and Electrical Engineering, University College London, London WC1E 7JE U.K. (e-mail: a.demosthenous@ucl.ac.uk)

This article has been accepted for publication in a future issue of this journal, but has not been fully edited. Content may change prior to final publication. Citation information: DOI 10.1109/OJVT.2022.3170522, IEEE Open Journal of Vehicular Technology

with MU-MIMO HB considering dual mobility of the Tx and Rx and achieving a root mean square (RMS) localization error of 6.30 m.

The rest of the paper is organized as follows. Section II undertakes a literature review to detail the existing mmWave and TDOA/FDOA localization techniques and their limitations. Section III details the localization with MU-MIMO HB and investigates the performances for BF and SM. In Section IV, CRB and CAF are estimated, following which emitter localization is undertaken; accuracy is improved by employing extended Kalman filtering. Concluding remarks are drawn in Section V.

II. Literature Review For Localization

A. Current mmWave Localization Techniques

The early work to obtain position and orientation in the context of mmWave technologies involves estimation and tracking of the AOA through beam-switching, user localization through hypothesis testing, and measurement of the received signal strength [4]-[7]. Various techniques employed for massive MIMO mmWave localization include estimating various parameters such as joint delay, AOA, and AOD, including hybrid techniques based on linearization and nonparametric kernel-based probabilistic models [8]-[12].

The large bandwidths in mmWave lead to much better temporal resolution, thus potentially improving the position estimates. More antenna elements in antenna arrays lead to smaller beamwidth with higher accuracy and resolution for the angular estimation. To leverage these characteristics, recent trends have focused on estimating position and orientation with a combination of AOA, AOD, and time of arrival (TOA). The CRB bounds of position and orientation for uniform linear arrays are derived in [13] by employing signals from a single transmitter (Tx), in line-of-sight (LOS), non-line-of-sight (NLOS), and obstructed-line-of-sight conditions for downlink localization. The closed-form of FIM is derived by employing geometric relationships for the channel, position, and orientation. For the non-uniform arrays, CRBs of position and orientation are given in [14]. For an indoor channel employing BF and SM, CRBs for TOA and AOA are derived in [15] using the CAF. The CRBs are compared for BF and SM for the single-user (SU)-MIMO case. In [13]-[15], it is further shown that the position and orientation estimates can benefit from NLOS components. However, the effects of Tx location, mobile terminal, and points of incidence of NLOS components are not analyzed for the presented results. The effects of NLOS components on position and orientation are given in [16]. It is shown that for sufficiently high temporal and spatial resolution, NLOS components provide position and orientation information which can increase the estimation accuracy. However, the accuracy depends on the number of NLOS paths that are not guaranteed in outdoor mmWave channels.

The aforementioned techniques are applied to static channels or when the Tx-Rx mobility is not quantified or depends on robust beam switching/control strategies for accurate AOD/AOA estimation. Most of the techniques apply to SU-MIMO, which does not leverage multiple vehicles present in a given area of interest. On the contrary, beam-tracking becomes onerous because more vehicles require robust, fast beam switching techniques. As a result, accurate AOD/AOA estimation becomes challenging and is prone to errors as Tx/Rx is mobile.

For the dynamic scenarios present in V2V channels, the Doppler shift measurements can provide additional Fisher information for localization [17]. One such technique is localization of the Tx with TDOA and FDOA estimation, which is employed in a wide range of applications for military, security and civilian use [18].

B. Comparison of Existing TDOA/FDOA Techniques

This section examines some of the main localization techniques based on TDOA/FDOA estimation. Localization based on TDOA estimation is suitable for high-bandwidth applications such as radars and mmWave V2V communication, while FDOA estimation can exploit the Doppler shifts in V2V communication [19], [20]. Localization with joint TDOA/FDOA estimation is a two-stage process. The first stage employs CAF to simultaneously estimate TDOA/FDOA from an emitter using maximum-likelihood methods [21]-[24]. Multiple TDOA/FDOA measurements are employed in the second stage to estimate the emitter location [25]. In [20], the approach aims to improve localization accuracy by nearing the CRB limits targeted at UAV applications by fusion of measurements when the likelihood of only one TDOA measurement is present; a likely scenario in a highly dynamic 3D UAV channel environment. Further, the Gaussian mixture presentation of measurements-integrated track splitting [26] filter is extended to adapt to the UAV channel for adequate tracking of the mobile emitter. Other techniques include reducing the computational requirements with algebraic [27], [28], and numerical solutions [29]. Techniques in the second stage include localization using satellites [30] and fixed sensor networks [31]. The two-stage localization accuracy depends on the signal-to-noise ratio (SNR), resulting in higher localization errors at low SNRs. On the other hand, single-stage techniques may be employed to reduce such errors in localization. Single-stage techniques known as direct position determination enable emitter localization directly from the CAF [32], [33].

The mentioned TDOA/FDOA based techniques either improve localization accuracy or reduce the computational requirements. However, the techniques are applied in simplistic or other scenarios not applicable to mmWave V2V channels.

III. Localization With MU-MIMO HB

A. MU-MIMO HB Localization

A 2-D geometrical scenario is given in Fig 1. The aim is to determine the location of the emitter vehicle *E,* using signals received by multiple user vehicles addressed as users. Henceforth each user is given as U_a, $a \in [1, V]$, where V is the total number of users. Since the CAF operates only on two received signals simultaneously, the users need to be paired. The assumption is made that the two users are time and frequency synchronized with each other, although not synchronized in any way with *E*.

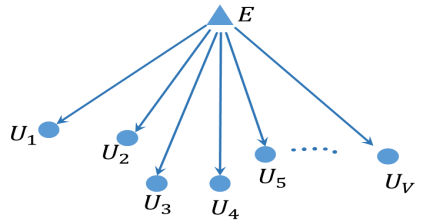

Fig. 1. Emitter localization in V2V.

Consider the m^{th} pair of users U_a and U_b where $a, b \in [1, V], a \neq b$ and $m \in [1, M]$. The TDOA $\tau_{a_m b_m}$ and FDOA $f_{a_m b_m}$ between the signals received by these users can be jointly estimated by the CAF. If the down-converted complex baseband signals received by U_a and U_b are $r_{a_m}(t)$ and $r_{b_m}(t)$ respectively, then CAF for the m^{th} pair is [21]:

$$\text{CAF}(\tau_{a_m b_m}, f_{a_m b_m}) = \int_0^T r_{a_m}(t) r_{b_m}^*(t + \tau_{a_m b_m}) e^{-j2\pi f_{a_m b_m} t} dt \quad (1)$$

where T is the integration time and '*' is the complex conjugate. The parameters $\tau_{a_m b_m}$ and $f_{a_m b_m}$ are required to be searched that cause simultaneously $|\text{CAF}(\tau_{a_m b_m}, f_{a_m b_m})|$ to peak. Due to different geometry between *E* and the various users, and the users having different quality of data, selecting a pair of users can be crucial in determining the location accuracy. Various strategies exist for user pairing. This could be based on whether the pairs share information or not; or given a set of users how to optimally choose pairing [34]. Ideally a complete set of users could be employed which although results in excessive data volume, can be alleviated as mmWave enables high-data rates. The emitter vehicle *E* employs a HB Tx where precoding is applied to both digital baseband and analog RF domains as in Fig. 2 [35]-[41]. The subscript *a* indicates for the U_a user where:

N_{U_a} is the number of signal streams

F_{BB_a} is the digital precoder

N_T number of antenna elements in the Tx array

$N_{RF_a}^T$: number of Tx RF chains/transceivers

F_{RF_a}: analog precoder of size $N_T \times N_{RF_a}^T$

N_{ds}: number of data streams

N_{R_a} number of antenna elements Rx array

$N_{RF_a}^R$: number of Rx RF chains/transceivers

W_{RF_a}: analog coder of size $N_{R_a} \times N_{RF_a}^R$

W_{BB_a}: digital coder of size $N_{RF_a}^R \times N_{U_a}$

The HB architecture can be partitioned into virtual sectors where each U_a has multiple signal streams N_{U_a}, one F_{BB_a}, and a number of RF chains/transceivers $N_{RF_a}^T$. This can be a fully connected or a partially connected architecture. A fully connected architecture is given in Fig. 2, where each RF chain is connected to all antenna elements in the Tx array. This full-connected scheme provides full beamforming gain per RF chain but with a high complexity of $N_T \times N_{RF_a}^T$ RF paths. For the partially-connected architecture, each of the RF chains is connected to $N_T / N_{RF_a}^T$ antenna elements in the Tx array. This partially-connected architecture leads to lower hardware complexity of RF paths at the cost of $1/N_{RF_a}^T$ BF gain. In both cases, the number of data streams N_{ds} that is transmitted for a user are given by $N_{RF_a}^T$. Joint spatial division multiplexing can be employed to determine F_{BB_a} and F_{RF_a} precoding weights for the selected system configuration [41]-[43]. Each user Rx array is composed of N_{R_a} number of antenna elements, an analog coder W_{RF_a}, $N_{RF_a}^R$ number of RF chains, and the digital coder W_{BB_a} resulting back in N_{U_a} signal streams.

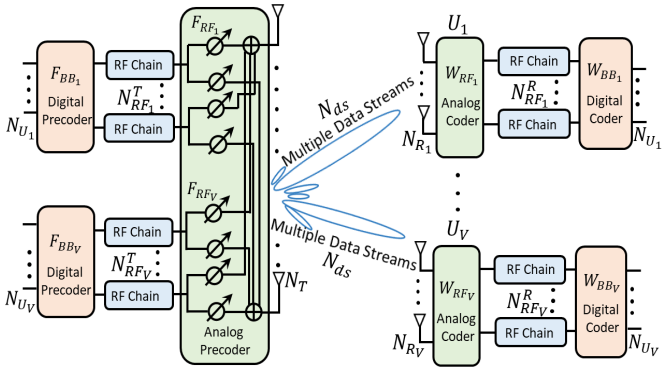

Fig. 2. MU-MIMO hybrid beamforming.

In high or sufficient SNR conditions, SM can be employed wherein multiple data streams are transmitted to each user. However, low SNR/cell edge conditions only allow a single data stream using the BF mode transmission. The down-converted complex baseband signal as received by U_a at time *t*, after propagating through the SM-MIMO channel is given by:

$$r_a(t) = \alpha_a \sum_{ds=1}^{N_{ds}} x_{ds}(t - \tau_a) e^{j(2\pi f_{d_a} t + \theta_{a,ds})} + w_a(t) \quad (2)$$

where the symbols are:

α_a : $\sqrt{P_a / N_{ds}}$ where, P_a is the signal power received,

x_{ds} : signal envelope of a randomly modulated symbol transmitted in a single data stream,

This article has been accepted for publication in a future issue of this journal, but has not been fully edited. Content may change prior to final publication. Citation information: DOI 10.1109/OJVT.2022.3170522, IEEE Open Journal of Vehicular Technology

τ_a : signal delay,
f_{d_a} : Doppler shift,
$\theta_{a,ds}$: random phase offset in one data stream, assumed to be uniformly distributed over $[0,2\pi]$,
w_a : white, zero-mean complex Gaussian noise,
ds : data stream number.

B. CRB for Multiple User Pairs

For a total of M pairs, the estimation parameter vector that is required to be estimated by the m^{th} pair of users is:

$$\phi_m = \left[\tau_{a_m b_m}, f_{a_m b_m}\right]^{\intercal}. \tag{3}$$

The maximum likelihood estimator $\hat{\phi}_m$ of the TDOA and FDOA are determined by solving the following optimization problem [21]:

$$\hat{\phi}_m = \underset{\tau_{a_m b_m}, f_{a_m b_m}}{\arg\max} \left|\mathrm{CAF}\left(\tau_{a_m b_m}, f_{a_m b_m}\right)\right|. \tag{4}$$

The FIM for ϕ_m is given by [21]:

$$J(\phi_m) = \begin{vmatrix} \frac{TB^3}{0.3025}\gamma_m & 0 \\ 0 & \frac{BT^3}{0.3025}\gamma_m \end{vmatrix} \tag{5}$$

where γ_m is the effective SNR given by:

$$\gamma_m = 2\frac{\gamma_{a_m}\gamma_{b_m}}{1+\gamma_{a_m}+\gamma_{b_m}}. \tag{6}$$

In (6) γ_{a_m} and γ_{b_m} are the SNRs in the respective user Rxs with the noise bandwidth B. The TDOA accuracy improves for larger signal bandwidths and FDOA accuracy improves for larger integration periods.

The FIM of $\boldsymbol{J_M}(\boldsymbol{\phi})$, for all the combined M user pairs where $\boldsymbol{\phi} = [\phi_1^{\intercal}, \phi_2^{\intercal} \ldots \phi_M^{\intercal}]^{\intercal}$ has a block structure, and is given by [34]:

$$\boldsymbol{J_M}(\boldsymbol{\phi}) = \begin{vmatrix} J(\phi_1) & I(\phi_{12}) & \cdots & I(\phi_{1M}) \\ I(\phi_{21}) & J(\phi_2) & \ddots & I(\phi_{2M}) \\ \vdots & \ddots & \ddots & \vdots \\ I(\phi_{M1}) & I(\phi_{M2}) & \ddots & J(\phi_M) \end{vmatrix} \tag{7}$$

where $I(\phi_{mn})$ is the cross-term FIM between m^{th} and n^{th} user pair. The cross-terms increase the computational requirement in the network. Since some users may be paired with more than one pair, their communication needs careful consideration to avoid a collision. When no user information is shared among other pairs the cross-term FIMs $I(\phi_{mn})$ are zero and the FIM reduces to:

$$\boldsymbol{J_M}(\boldsymbol{\phi}) = \begin{vmatrix} J(\phi_1) & 0 & \cdots & 0 \\ 0 & J(\phi_2) & \ddots & 0 \\ \vdots & \ddots & \ddots & \vdots \\ 0 & 0 & & J(\phi_M) \end{vmatrix}. \tag{8}$$

Although the FIM in (8) requires fewer computations than (7), it may yield higher localization errors due to fewer entries in the FIM. The dividend for sharing information between pairs needs careful consideration due to the increase in computation, network capacity, and latency. In this paper, it is assumed that no information is shared between any user pairs.

C. Spatial Multiplexing and Beamforming

SM is likely to be employed in high SNR conditions to improve the network capacity wherein the channel can support multiple data streams to each user. SM increases the number of $x_{ds}(t)$ that are demodulated for each user since $ds \in \{1, N_{ds}\}$ where $ds > 1$ for SM. Accordingly, for SM the resulting CAF in (1) is dependent on more than one $x_{ds}(t)$ in (2) for each user. Accurate estimation of $\hat{\phi}_m$ for $ds > 1$ is therefore dependent on the random nature of $\theta_{i,ds}$ in (2) and how coherent is the summation of all $x_{ds}(t)$ present in the data stream. This can result in spurious peaks rather than a single peak for a given CAF, thereby reducing the accuracy of $\hat{\phi}_m$. Therefore, even in the absence of noise and high SNR conditions, the peak of the CAF may not correspond to the true TDOA/FDOA, thereby reducing the accuracy of localization. If $x_{ds}(t)$ are assumed as unit vectors, then amplitude (A) of the squared envelope of a sum of these unit vectors, with random phases has a probability density function given by [44]:

$$p(A) = \begin{cases} \frac{1}{N_{ds}-1} exp\left(-\frac{A+1}{N_{ds}-1}\right) I_0\left(\frac{2\sqrt{A}}{N_{ds}-1}\right); & A \geq 0 \\ 0; & \text{otherwise.} \end{cases} \tag{9}$$

where $I_0(.)$ is the first-order modified Bessel function, and $N_{ds} > 2$. For $N_{ds} = 2$ $p(A)$ is very high $\rightarrow \infty$ [44]. Fig. 3 indicates the probability of all $x_{ds}(t)$ in the data stream being summed up coherently. The probability of three $x_{ds}(t)$ being coherently summed up is given by $N_{ds} = 3$ and $A = 9$ which is $p(A) = 0.0164$. This reduces to 0.004 for four $x_{ds}(t)$ i.e. at $N_{ds} = 4$ and $A = 16$. Likewise the probability of more than four $x_{ds}(t)$ coherently summing up is even lower. Therefore, the likelihood of CAF having spurious peaks increases for SM which has more than one $x_{ds}(t)$ in one data stream. In comparison, in BF the CAF output estimates are based on a single $x_d(t)$ for each user. Therefore, even in the presence of noise and low SNR conditions the peak of the CAF is more likely to correspond to the true TDOA/FDOA.

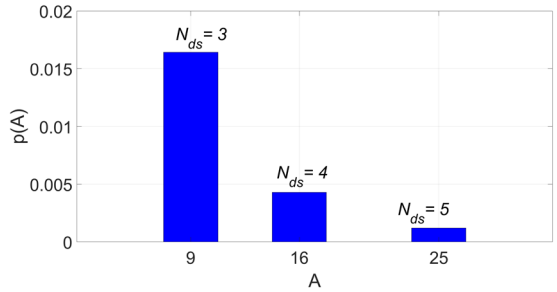

Fig. 3. Probability density function values for squared envelop of a sum of random phase vectors for different data streams.

IV. Emitter Localization

A. MmWave 3D Statistical Spatial Channel Model

The mmWave channel simulator employed in this paper is based on a 3D statistical spatial channel model for urban LOS and NLOS channels developed from extensive 28 GHz, 60 GHz, 73 GHz, and 140 GHz ultra-wideband propagation measurements in the cities of New York City and Austin, USA [45], [46]. The model generates channel impulse responses that match measured field data at a wide range of distances from 10-10,000 m and over local areas based on the time cluster-spatial lobe modeling framework. The approach extends the 3GPP model through the directional RMS lobe angular spreads and is consistent with the 3GPP modeling framework. Based on the 3D statistical channel model in [45], [46], a MATLAB-based statistical simulator, NYUSIM, has been developed by New York University [47] that can generate 3D AOD and AOA power spectra along with omnidirectional and directional power delay profiles that match measured field results [48]. 3GPP assumes an unrealistically large number of strong eigenvalues of the channel matrix, which are not found in mmWave channels [49]. Accordingly, NYUSIM is employed in this paper to simulate the MIMO channel for more realistic results [50].

NYUSIM employs spatial consistency to simulate the time-variant channel along the user trajectory. Due to the high correlation of a wireless channel over a distance of 10-15 m, incorporating spatial consistency is required to accurately represent the consecutive and spatially correlated channel evolution along the user movement in a local area. The channel update has two parts viz., large-scale parameters such as shadow fading, LOS/NLOS condition, and small-scale parameters such as the power, delay, phase and angles of each multipath component. The large-scale parameters are updated by using a spatially-correlated map, and the small-scale parameters are updated by a geometry-based reflection surface [48].

B. Estimating CRB

From (8), for a constant bandwidth B and integration time T, the effective SNRs γ_m were obtained for 100 repetitive runs with NYUSIM to simulate the CRB of ϕ_m for BF and SM. The simulation specifications are given in Table I. BF corresponds to one data stream and SM corresponds to two or four data streams. The user positions were obtained from NYUSIM randomly in the distance interval [10, 500] m from E for each simulation run as given in Fig. 4 for 10 user pairs.

A vehicle-mounted base station (VMB) was assumed for E. VMBs offer advantages such as real-time communication, employing massive MIMO technology and dynamic caching; and therefore, proposed as a suitable option for mmWave V2V communication [51]. The extremely high frequencies (mmWave/THz) in these bands on interest motivate design of VMBs as compact size arrays with very fine pencil beams. At E, $N_T = 256$ and for users $N_{R_a} = 4$, meaning that at most 64 users can be simultaneously supported by E which can form at most 32 user pairs. In addition, the user can receive at most four different data streams from E. Thus, 10, 20, and 30 user pairs and 1, 2, 4 data streams in the channel simulations were chosen.

TABLE I
MmWave Channel Specifications

Parameters	Values
Carrier frequency	73 GHz
RF bandwidth (B)	800 MHz
Scenario	UMi LOS
Tx-Rx separation distance	Uniform [50, 100] m
User moving direction	Uniform [0, 360]º
User Velocity	[5, 10, 15, 20] m/s
Transmit power	10 W
Emitter (E) height	1.5 m
User height	1.5 m
Emitter (E) antenna	16 x 16 URA
User antenna	2 x 2 URA
Integration time (T)	1 ms
Number of user pairs (M)	[10, 20, 30]
Number of data streams (N_{ds})	[1, 2, 4]

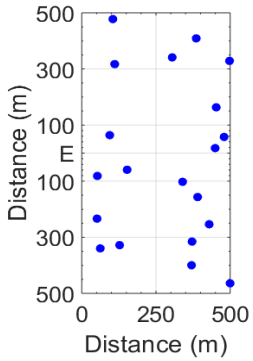

Fig. 4. Random user positions in the interval [10, 500] m from E

The normalized CRBs of ϕ_m for various number of user pairs and data streams are plotted in Fig. 5, indicating that BF has a lower CRB than SM. This agrees with the earlier analysis for BF and SM provided by (9) and Fig. 3. SM with four data streams with 10 pair of users produce the worst performance. The yellow bar for SM, $N_{ds} = 4$ with 10 user pairs is 0 dB and therefore not visible. Furthermore, Fig.5 shows that increasing the number of user pairs lowers the CRB for both BF and SM. Therefore, the high number of users likely to be present in V2V communication with MU-MIMO HB can be leveraged.

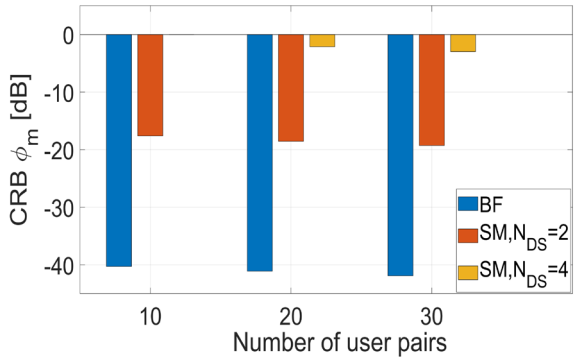

Fig. 5. The normalized CRBs of ϕ_m.

This article has been accepted for publication in a future issue of this journal, but has not been fully edited. Content may change prior to final publication. Citation information: DOI 10.1109/OJVT.2022.3170522, IEEE Open Journal of Vehicular Technology

C. Estimating $\hat{\phi}_m$

TDOA and FDOA i.e. $\tau_{a_m b_m}$ and $f_{a_m b_m}$ are estimated by integrating the received signals of a pair of users from the same E and calculating CAF given in (1). The estimated $\tau_{a_m b_m}$ and $f_{a_m b_m}$ give the largest absolute value of CAF in (4). The channel specifications are listed in Table I. The parameters of the transmitted signals are given in Table II. The normalized absolute CAF values with N_{ds} = 1, 2 and 4 at 10 dB and -20 dB SNR are shown in Fig. 6 and Fig. 7, respectively. It can be observed that the estimated $\tau_{a_m b_m}$ and $f_{a_m b_m}$ for BF and SM are almost identical at 10 dB SNR. As SNR decreases, the estimation performance degrades, especially for the SM case. At -20 dB SNR the twin peaks for the CAF are visible for $N_{ds} \geq 2$, indicating the formation of spurious peaks, which reduces the accuracy of TDOA/FDOA estimation.

TABLE II
MMWAVE SIGNAL PARAMETERS

Parameters	Values
Modulation	OFDM 256 QAM
Bit rate	10 Mbps
Samples per symbol	16
Transmitter filter	sinc pulse shaping
SNR	[0, -10, -20] dB

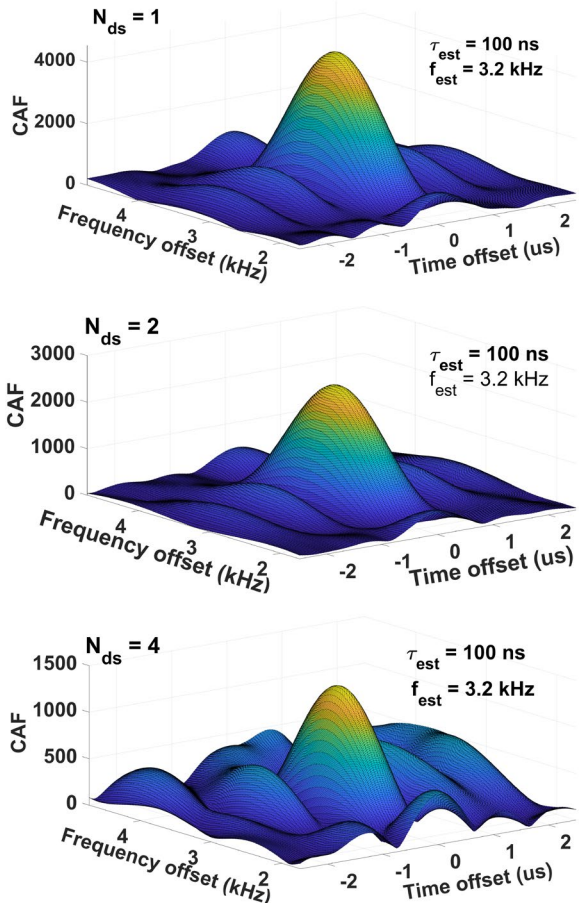

Fig. 6 CAF with 1, 2, 4 data streams with 10 dB SNR.

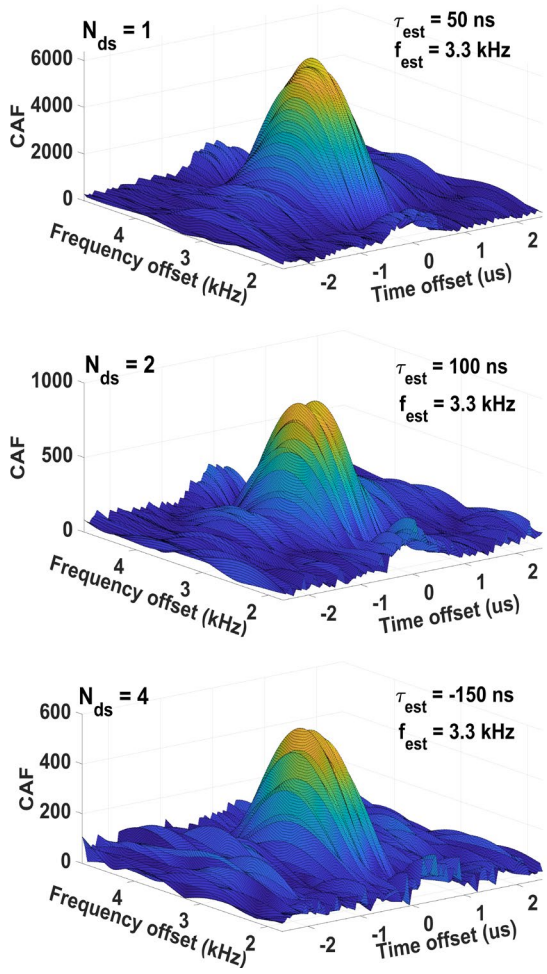

Fig. 7. CAF with 1, 2, 4 data streams with -20 dB SNR.

D. Localization Performance

For the two-stage localization on estimating $\tau_{a_m b_m}$ and $f_{i_m j_m}$ from the CAF matrix, the location of E can be calculated by solving a system of non-linear equations which [52]:

$$\tau_{a_m b_m}(x_e, y_e) = \frac{1}{c}\left(\sqrt{(x_{m,1} - x_e)^2 + (y_{m,1} - y_e)^2} - \sqrt{(x_{m,2} - x_e)^2 + (y_{m,2} - y_e)^2}\right) \quad (10)$$

$$f_{a_m b_m}(x_e, y_e) = \frac{f_c}{c}\left(\frac{v_{x,1}(x_{m,1} - x_e) + v_{y,1}(y_{m,1} - y_e)}{\sqrt{(x_{m,1} - x_e)^2 + (y_{m.1} - y_e)^2}} - \frac{v_{x,2}(x_{m,2} - x_e) + v_{y,2}(y_{m,2} - y_e)}{\sqrt{(x_{m,2} - x_e)^2 + (y_{m,2} - y_e)^2}}\right) \quad (11)$$

This article has been accepted for publication in a future issue of this journal, but has not been fully edited. Content may change prior to final publication. Citation information: DOI 10.1109/OJVT.2022.3170522, IEEE Open Journal of Vehicular Technology

where $x_{m,1}, y_{m,1}$ and $x_{m,2}, y_{m,2}$ are the location of the user pairs. x_e, y_e is the location of E to be estimated; f_c, v are the carrier frequency and user velocity, respectively.

Ten user pairs with $N_{ds} = 1, 2$ and 4 data streams were used to estimate the location of the E. By setting the received SNR as 10 dB, the estimated $\tau_{a_m b_m}$ and $f_{a_m b_m}$ are almost identical for three different number of data streams, thus outputting an identical estimated location of E. The mmWave channel simulator NYUSIM provides time-variant channel conditions in spatial consistency mode to update the user location and channel condition. The spatial consistency parameters and user velocity settings for NYUSIM are given in Table III.

TABLE III
SPATIAL CONSISTENCY SETTINGS

Spatial Consistency Parameters	Values
Shadow fading correlation distance	10 m
LOS/NLOS correlation distance	15 m
User track type	Linear
Update distance	1 m
RX moving distance	30 m
Rx velocity	10 m/s
Rx moving direction	Uniform (0, 360) degree
Emitter moving distance	15 m
Emitter velocity	5 m/s
Emitter moving direction	0 degree (east)

Channel snapshots were generated every one meter, and a 15 m moving trajectory of the emitter was simulated for 16 users (corresponding to 8 user pairs). The median value of the estimated location obtained from 8 user pairs were used as the final estimated location of E at each time instance. The 15 estimated locations along the 15 m trajectory are plotted in Fig. 8, where most localization errors are within 15 m. In addition, there is no spatial correlation between two consecutive estimations. To further improve the localization performance and take spatial correlation into account, an extended Kalman filter was applied in the following section.

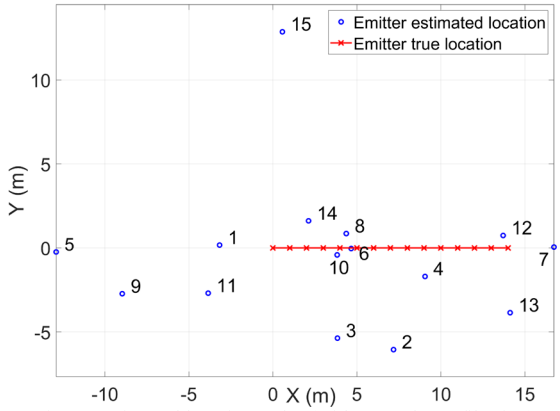

Fig. 8. Estimated locations of E (without Kalman filtering).

E. Reducing Localization Errors With Kalman Filtering

In addition to $\theta_{a,ds}$ and the number of $x_{ds}(t)$, another factor on which CAF depends is the received signal power α_a in (2). This can vary significantly due to scattering behavior of the mmWave channel leading to an increase in localization errors. The effect can be observed by the signal power received even for a slow-moving Tx. The power received for a Tx with a velocity of 5 m/s is shown in Fig. 9,

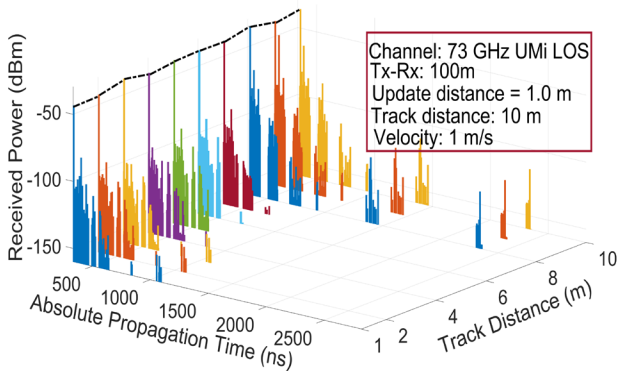

Fig. 9. Signal power received.

wherein the power received varies about 4.6 dB between 2 m and 3 m.

Kalman filters employ a series of measurements observed over time, containing statistical noise and other inaccuracies, and produce estimates of unknown variables that tend to be more accurate than those based on a single measurement alone [53]. The extended Kalman filter [54] can be employed for non-linear state-space models. In addition, the extended Kalman filter is highly accurate in estimation performance and has low computational complexity compared to, for example, particle filters and the unscented Kalman filter. Additionally, the performance of the EKF and the particle filter was found to be similar in [55]. The accuracy of localization in mmWave channels can be improved by employing extended Kalman filter to the estimated channel parameters, such as signal strength, DOA, and TOA [7], [56]. The state of the system is the position of $E(x, y)$ (ideally, it is (0, 0)), and the measurements are the TDOA and FDOA of each user pair. The state dynamics can be written as [57]:

$$x_k = Ax_{k-1} + w_k, \tag{12}$$

where x_k is the state vector of the position and velocity of the emitter (i.e., $(x_e, y_e, v_{x,e}, v_{y,e})$). To model the change in the emitter state vector caused by the constant velocity of the emitter, the transition matrix A is given by [57]:

$$\begin{bmatrix} 1 & 0 & dt & 0 \\ 0 & 1 & 0 & dt \\ 0 & 0 & 1 & 0 \\ 0 & 0 & 0 & 1 \end{bmatrix}$$

w_k is the process noise and is given by:

This article has been accepted for publication in a future issue of this journal, but has not been fully edited. Content may change prior to final publication. Citation information: DOI 10.1109/OJVT.2022.3170522, IEEE Open Journal of Vehicular Technology

$$\left[\frac{dt^2}{2} w_{a,x} \quad \frac{dt^2}{2} w_{a,y} \quad dt\, w_{a,x} \quad dt\, w_{a,y}\right]^t$$

where $w_{a,x}$ and $w_{a,y}$ are the random Gaussian accelerations in the x and y directions, respectively. In this study, it is assumed that the random accelerations in the x and y directions have a mean of 0 and a standard deviation of σ_w = 9 m/s^2 .

An extended Kalman filter includes two processing steps: prediction and update. The prediction step predicts the next state and covariance matrix based on the current state and current covariance matrix. It uses the defined transition matrix and process noise covariance matrix, given by [57]:

$$\tilde{x}_k = A\tilde{x}_{k-1} \tag{13}$$

$$\tilde{P}_k = A\tilde{P}_{k-1}A^T + Q \tag{14}$$

where Q is the noise covariance matrix, i.e. $E[w_k w_k^T]$. The Q matrix is given by [57]:

$$Q = \begin{bmatrix} \frac{T^4}{4} & 0 & \frac{T^3}{2} & 0 \\ 0 & \frac{T^4}{4} & 0 & \frac{T^3}{2} \\ \frac{T^3}{2} & 0 & \frac{T^2}{2} & 0 \\ 0 & \frac{T^3}{2} & 0 & \frac{T^2}{2} \end{bmatrix} \sigma_w^2 \tag{15}$$

assuming the random acceleration in the x and y direction ($w_{a,x}$ and $w_{a,y}$) are uncorrelated. The P matrix was initialized as the identity matrix since no prior knowledge of the accuracy of the initial estimate of the emitter position and velocity was assumed. The second step updates (or refines) the predicted state based on the measurements conducted at each time instance. The EKF observation model describes how the measured TDOA and FDOA are related to the position and velocity of the user. The relationship is provided in (18), (19). The user state is refined using the observation model (and the measured TDOA and FDOA). The Kalman gain is expressed as:

$$K = PH^T(HPH^T + R)^{-1} \tag{16}$$

where R is the uncertainty matrix of the TDOA and FDOA measurements. R is calculated from the variance of the measurement error between the ideal TDOA, FDOA and the measured TDOA, FDOA. H is the Jacobian matrix of the measurements with respect to the predicted state $\tilde{x}_k$, given by:

$$H = \begin{bmatrix} \frac{\partial \tau_{ij}}{\partial x} & \frac{\partial \tau_{ij}}{\partial y} \\ \frac{\partial f_{ij}}{\partial x} & \frac{\partial f_{ij}}{\partial y} \end{bmatrix}. \tag{17}$$

The updated $\hat{x}_k$ can be estimated by:

$$\hat{x}_k = \tilde{x}_k + Kv_k \tag{18}$$

where v_k is the difference between the measured TDOA and FDOA and the values of TDOA and FDOA predicted using the updated $\tilde{x}_k$ in (13), (14).

$$P_k = (I - KH)P_{k-1}. \tag{19}$$

For Tx mobility, a geometry-based channel evolution for the LOS path was employed. The emitter moved towards the east at 5 m/s from [0, 0]. Each Rx was located from 10 to 50 m away from E at 10 m/s in an arbitrary direction. 16 Rxs were simulated, forming eight user pairs. The updated Kalman filter with emitter mobility was applied, resulting in a RMS error of 6.5 m as shown in Fig. 10. The corresponding close up plot is depicted in Fig. 11. Note that the channel measurements used to characterize the localization performance with the Kalman filter and obtain Fig. 10 and 11 are identical to the channel measurements used for emitter localization without the Kalman filter, used to create Fig. 8.

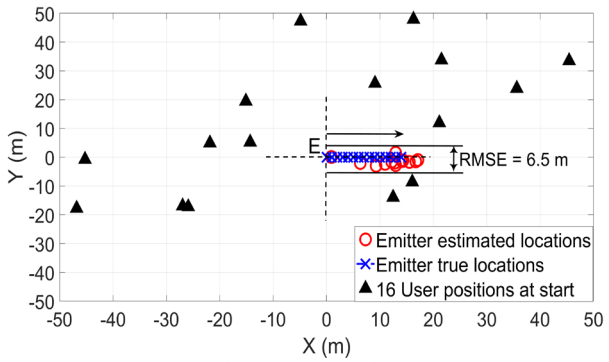

Fig. 10. Estimated locations of E after applying EKF.

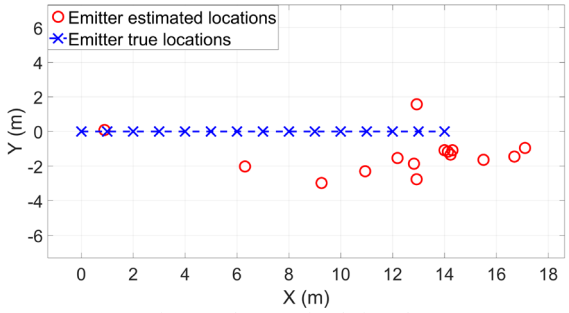

Fig. 11. Close up simulation plot. .

F. Discussion

Joint TDOA/FDOA estimation under the challenging conditions in V2V channels are potential candidates for localization estimates. The effects on various precoders or other non-ideal conditions such as imperfect CSI on accurate TDOA/FDOA estimation and localization could be an area for future work, along with strategies that could enable integration of the AOA/AOD estimates. Since all users have to transmit their received signals to a site which could be one

of the users or a dedicated base station in the network, this site handles a large amount of computations. Strategies need to be in place for reducing and balancing the computational load on the network. In case of data loss, the system localization processing will result in poor stability and increase in latency. To circumvent these issues distributed data compression could be employed to reduce the amount of data transmission, and distributed computations to reduce the computational load on site [58].

The existing MIMO localization methods together with this work are listed in Table IV. The localization errors are indicated as mean, RMS, position error bound (PEB) and probability of sub-meter accuracy.

TABLE IV
MIMO LOCALIZATION METHODS

References	MmWave Channel /Frequency/Bandwidth	Tx/Rx Mobility	Localization Error
[5]	Yes/38 GHz/Not given	No	Not given
[6]	Indoor/60 GHz/1.2 GHz	No	~1.5 m (Mean)
[8]	No/2 GHz/2.5 MHz	134 m/s	$< 10^{-1}$ m (RMS)
[9]	Yes/60 GHz/20-500MHz	No	$< 10^{-4}$ m (PEB)
[10]	No/Not Given/Not Given	No	~10-15 m (RMS)
[11]	No/7 GHz/30 MHz	No	~ 1 m *
[12]	No/Not Given/Not Given	No	~ 2 m (MSE)
[13]	Indoor/60 GHz/100 MHz	No	~0.14 m (LE)
[14]	Yes/38 GHz/125 MHz	No	~ 0.4 m (PEB)
[15]	Yes/60 GHz/1GHz	No	10^{-4}-10^{-3} m (PEB)
[16]	Yes/38 GHz/125 MHz	No	0.04-0.2 m (PEB)
This work	Yes/73 GHz/800 MHz	5-20 m/s	~6.3 m (RMS)

*Given as probability of sub-meter accuracy.

V. CONCLUSION

This paper has proposed a joint TDOA/FDOA estimation approach with MU-MIMO HB for mmWave V2V localization. At 10 dB SNR both SM and BF result in comparable localization errors. At lower SNR values, SM leads to larger errors compared to BF due to spurious peaks in the CAF. Due to the non-linear nature of the involved state-space models, the accuracy of estimation and tracking can be improved by employing an extended Kalman filter, resulting in a localization RMS error of ~6.3 m. The proposed technique resulted in a smaller user range error than the broadcasting GPS signal standard of ≤7.8 m with a 95% probability given by the US government [59].

Further efforts to improve the localization accuracy could look into the optimal user pairing strategy. Due to different propagating conditions, users will have different data quality as the geometry between users and the emitter plays a key role in determining the location accuracy. Pairing strategies and the trade-off in terms of accuracy and timeline requirements could be quantified. Strategies for optimal pairing and network load balancing could be employed with machine learning/AI and integrated to improve localization accuracy further.

REFERENCES

[1] T. S. Rappaport, et al., "Millimeter wave mobile communications for 5G cellular: It will work," *IEEE Access*, vol. 1, pp. 335-349, May 2013, doi: 10.1109/ACCESS.2019.2921522.

[2] *5G; Study on channel model for frequencies from 0.5 to 100 GHz*, 3GPP TR 38.901 Release 14 V14.1.0 (2017). Accessed Nov 11, 2020. [Online]. Available at: https://www.etsi.org/deliver/etsi_tr/138900_138999/138901/14.00.00_60/tr_138901v140000p.pdf

[3] J. Choi et al., "Millimeter-wave vehicular communication to support massive automotive sensing," *IEEE Commun. Mag*., vol. 54, no. 12, pp. 160-167, Dec. 2016, doi:10.1109/MCOM.2016.1600071CM.

[4] P. Sanchis, et al., "A novel simultaneous tracking and direction of arrival estimation algorithm for beam-switched base station antennas in millimeter-wave wireless broadband access networks," in *Proc. IEEE Antennas Propag. Soc. Int. Symp.*, San Antonio, TX, USA, Jun. 2002, pp. 594-597, doi: 10.1109/APS.2002.1016415. .

[5] H. Deng and A. Sayeed, "Mm-wave MIMO channel modeling and user localization using sparse beamspace signatures," in *Proc. Int. Workshop Signal Process. Adv. Wireless Commun. (SPAWC)*, Toronto, ON, Canada, Jun. 2014, pp. 130-134, doi: 10.1109/SPAWC.2014.6941331.

[6] M. Vari and D. Cassioli, "MmWave RSSI indoor network localization," in *Proc. Int. Conf. Commun. (ICC)*, Sydney, NSW, Australia, Jun. 2014, pp. 127-132, doi: 10.1109/ICCW.2014.6881184.

[7] O. Kanhere and T. S. Rappaport, "Position Locationing for Millimeter Wave Systems," *2018 IEEE Global Communications Conference (GLOBECOM)*, Abu Dhabi, United Arab Emirates, 2018, pp. 206-212

[8] A. Hu, et al., "An ESPRIT-based approach for 2-D localization of incoherently distributed sources in massive MIMO systems," *IEEE J. Sel. Topics Signal Process.*, vol. 8, no. 5, pp. 996-1011, Mar. 2014, doi: 10.1109/JSTSP.2014.2313409.

[9] A. Guerra, et al., "Position and orientation error bound for wideband massive antenna arrays," in *Proc. Int. Conf. Commun. Workshop (ICC)*, London, U.K., Jun. 2015, pp. 853-858, doi: 10.1109/ICCW.2015.7247282.

[10] V. Savic and E. G. Larsson, "Fingerprinting-based positioning in distributed massive MIMO systems," in *Proc. IEEE Veh. Technol. Conf. (VTC)*, Boston, MA, USA, Sep. 2015, pp. 1-5, doi: 10.1109/VTCFall.2015.7390953.

[11] N. Garcia, et al., "Direct localization for massive MIMO," *IEEE Trans. Signal Process.*, vol. 65, no. 10, pp. 2475-2487, May 2017, doi: 10.1109/TSP.2017.2666779.

[12] J. Li, et al., "Position location of mobile terminal in wireless MIMO communication systems," *J. Commun. Netw.*, vol. 9, no. 3, pp. 254-264, Sep. 2007, doi: 10.1109/JCN.2007.6182853.

[13] A. Shahmansoori, et.al., "Position and orientation estimation through millimeter-wave MIMO in 5G systems," *IEEE Trans. Wireless Commun*., vol. 17, no. 3, pp. 1822-1835, Mar. 2018, doi : 10.1109/TWC.2017.2785788.

[14] Z. Abu-Shaban, et al., "Error bounds for uplink and downlink 3D localization in 5G mmWave systems," *IEEE Trans. Wireless Commun.*, vol. 17, no. 8, pp. 4939-4954, Aug. 2018, doi: 10.1109/TWC.2018.2832134.

[15] A. Guerra, et al., " Single-anchor localization and orientation performance limits using massive arrays: MIMO vs. beamforming," *IEEE Trans. Wireless Commun.*, vol. 17, no. 8, pp. 5241–5255, Aug. 2018, doi : 10.1109/TWC.2018.2840136.

[16] R. Mendrzik, et.al., "Harnessing NLOS components for position and orientation estimation in 5G millimeter-wave MIMO," *IEEE Trans. Wireless Commun*., vol. 18, no.1, pp. 93-107, Jan. 2019, doi: 10.1109/TWC.2018.2877615.

[17] Y. Han et al., "Performance Limits and Geometric Properties of Array Localization," *IEEE Trans. Info. Theory*, vol. 62, no. 2, pp. 1054-1075, Feb. 2016, doi: 10.1109/TIT.2015.2511778.

[18] V.L. Do, "TDOA-based passive tracking of multiple civilian applications," in Proc. *IEEE Int. Conf. Signal Proc. Commun. Syst.*, pp. 234-245, Dec. 2019, doi: 10.1109/ICSPCS47537.2019.9008710.

[19] B. Friedlander, "A passive localization algorithm and its accuracy analysis," *IEEE J. Ocean Eng*. vol. 12, no. 1, pp. 234-245, Jan. 1987, doi: 10.1109/JOE.1987.1145216.

[20] D. Musicki, et al., "Mobile E geolocation and tracking using TDOA and FDOA measurements," *IEEE Trans. Signal Process*., vol. 58, no. 3, pp. 1863-1874, Mar. 2010, doi: 10.1109/TSP.2009.2037075.

[21] S. Stein, "Algorithms for ambiguity function processing," *IEEE Trans. Acoust., Speech Signal Process*., vol. ASSP-29, no. 3, pp. 588-599, Jun. 1981, doi: 10.1109/TASSP.1981.1163621.

[22] S. Stein, "Differential delay/Doppler ML estimation with unknown signals," *IEEE Trans. Signal Process*., vol. 41, no. 8, pp. 2717-2719, Aug. 1993, doi: 10.1109/78.229901.

[23] R. Bardelli, et al., "Interference localization for the Eutelsat satellite system," in *Global Telecommun. Conf., GLOBECOM'95*, Singapore, Nov. 1995, vol. 3, pp. 1641–1651, doi: 10.1109/GLOCOM.1995.502690.

[24] DG Kim, et al., "Computationally efficient TDOA/FDOA estimation for unknown communication signals in electronic warfare systems," IEEE Trans. Aero. Elect. Syst., vol. 54, no. 1, pp. 44-47, Aug 2017, doi: 10.1109/TAES.2017.2735118.

[25] G. Wang, et al., "A bias-reduced non-linear WLS method for TDOA/FDOA-based source localization," *IEEE Trans. Veh. Tech*., vol. 65, no. 10, pp. 8603 - 8615, Oct 2016, doi: 10.1109/TVT.2015.2508501.

[26] D. Musicki and R. Evans, "Measurement Gaussian sum mixture target tracking," in 9th *Int. Conf. Inf. Fusion*, Florence, Italy, Jul. 2006.

[27] A. Noroozi, et al., "Improved algebraic solution for source localization from TDOA and FDOA measurements," *IEEE Wireless Commun*. Lett., vol. 7, no. 3, pp. 352 - 355, Jun. 2018, doi: 10.1109/LWC.2017.2777995.

[28] K. Ho and W. Xu, "An accurate algebraic solution for moving source location using TDOA and FDOA measurements," *IEEE Trans. Signal Process.*, vol. 52, no. 9, pp. 2453-2463, Sep. 2004, doi: 10.1109/TSP.2004.831921.

[29] H. Yu, et al., "An efficient constrained weighted least squares algorithm for moving source location using TDOA and FDOA measurements," *IEEE Trans. Wireless Commun*., vol. 11, no. 1, pp. 44-47, Jan. 2012, doi: 10.1109/TWC.2011.102611.110728.

[30] K. Lee, et al., "TDOA/FDOA based adaptive active target localization using iterated dual-EKF algorithm," *IEEE Commun. Lett*., vol. 23, no. 4, pp. 752 - 755, Apr. 2019, doi: 10.1109/LCOMM.2019.2899615.

[31] X. Zhang, et al., "Maximum likelihood and IRLS based moving source localization with distributed sensors," *IEEE Trans. Aero. Elect. Sys*., vol. 57, no. 1, pp. 448 - 461, Feb. 2021, doi: 10.1109/TAES.2020.3021809.

[32] A. Weiss and A. Amar, "Direct geolocation of stationary wide band radio signal based on delays and Doppler shifts," *IEEE Workshop Stat. Signal Process*., Aug. 31-Sept. 3, 2009, Cardiff, Wales, UK, doi: 10.1109/SSP.2009.5278630.

[33] N. Vankayalapati and S. Kay, "Asymptotically optimal localization of an emitter of low probability of intercept signals using distributed sensors," *IEEE Trans. Aero. Elect. Sys.,* vol. 48, no. 1, pp. 737-748, Jan. 2012, doi: 10.1109/TAES.2012.6129667.

[34] X. Hu and M. Fowler, "Sensor selection for multiple sensor emitter location systems," *in Proc. IEEE Aero. Conf*., May 2008, pp.1-10, doi: 10.1109/AERO.2008.4526431

[35] L. Liang, et al., "Low-complexity hybrid precoding in massive multiuser MIMO systems," *IEEE Wireless Commun. Lett*., vol. 3, no. 6, pp. 653-656, Dec. 2014, doi: 10.1109/LWC.2014.2363831.

[36] A. Alkhateeb, et al., "Limited feedback hybrid precoding for multiuser millimeter wave systems," *IEEE Trans. Wireless Commun*., vol. 14, no. 11, pp. 6481-6494, Nov. 2015, doi: 10.1109/TWC.2015.2455980.

[37] Y. Ren, et al., "Multiple-beam selection with limited feedback for hybrid beamforming in massive MIMO systems," *IEEE Access*, vol. 5, pp. 13327-13335, Feb. 2017, doi: 10.1109/ACCESS.2017.2666782.

[38] C. B. Peel, et al., "A vector perturbation technique for near-capacity multiantenna multiuser communication-Part I: Channel inversion and regularization," *IEEE Trans. Commun*., vol. 53, no. 1, pp. 195-202, Jan. 2005, doi: 10.1109/TCOMM.2004.840638.

[39] W. Ni and X. Dong, "Hybrid block diagonalization for massive multiuser MIMO systems," *IEEE Trans. Commun*., vol. 64, no. 1, pp. 201–211, Jan. 2016, doi: 10.1109/TCOMM.2015.2502954.

[40] R. Rajashekar and L. Hanzo, "Iterative matrix decomposition aided block diagonalization for mm-Wave multiuser MIMO systems," *IEEE Trans. Wireless Commun*., vol. 16, no. 3, pp. 1372–1384, Mar. 2017, doi: 10.1109/TWC.2016.2628357.

[41] Z. Li , et.al., "Hybrid beamforming design for millimeter-wave multiuser massive MIMO downlink." In *Proc. IEEE Int. Conf. Commun., ICC* 2016, Malaysia, May 2016, doi: 10.1109/ICC.2016.7510845.

[42] A. Adhikary et.al., "Joint spatial division and multiplexing - The large-scale array regime." *IEEE Trans. on Info. Theory*, vol. 59, no. 10, pp. 6441-6463, Oct. 2013, doi: 10.1109/TIT.2013.2269476.

[43] Q. Spencer et. al., "Zero-forcing methods for downlink spatial multiplexing in multiuser MIMO channels." *IEEE Trans. on Signal Process*., vol. 52, no. 2, pp. 461-471, Feb. 2004, doi: 10.1109/TSP.2003.821107.

[44] M. Simon, "On the probability density function of the squared envelop of a sum of random phase vectors," *IEEE Trans. Commun.*., vol. 33, no. 9, pp. 993-996, Sep. 1985.

[45] M. K. Samimi and T. S. Rappaport, "3-D millimeter-wave statistical channel model for 5G wireless system design," *IEEE Trans. Microw. Theory Techn.*, vol. 64, no. 7, pp. 2207-2225, Jul. 2016, doi: 10.1109/TMTT.2016.2574851.

[46] T. S. Rappaport, et al., "Wideband millimeter-wave propagation measurements and channel models for future wireless communication system design," *IEEE Trans. Commun*., vol. 63, no. 9, pp. 3029-3056, Sep. 2015, doi: 10.1109/TCOMM.2015.2434384.

[47] NYU Simulator, NYU Wireless, NYU. Accessed Dec 08, 2020. [Online]. Available at: https://wireless.engineering.nyu.edu/nyusim/

[48] S. Sun, et al., "A novel millimeter-wave channel simulator and applications for 5G wireless communications," in *Proc. IEEE Int. Conf. on Commun., (ICC)*, Paris, 2017, pp. 1-7, doi: 10.1109/ICC.2017.7996792.

[49] S. Sun, et al., "Propagation models and performance evaluation for 5G millimeter-wave bands," in *IEEE Trans. on Veh. Tech*., vol. 67, no. 9, pp. 8422-8439, Sept. 2018, doi: 10.1109/TVT.2018.2848208.

[50] S. Ju and T. S. Rappaport, "Millimeter-wave extended NYUSIM channel model for spatial consistency," in *Proc. IEEE Global Commun. Conf. (GLOBECOM)*, Abu Dhabi, United Arab Emirates, 2018, pp. 1-6, doi: 10.1109/GLOCOM.2018.8647188.

[51] C. Li, et al., "Vehicle-mounted base station for connected and autonomous vehicles: opportunities and challenges," *IEEE Wire. Commun. Mag.*, vol. 26, no. 4, pp. 30-36, Aug. 2010, doi: 10.1109/MWC.2019.1800541.

[52] Jacob I. Overfield, "Impact of MIMO Transmission on CAF-based Geolocation", MS thesis, May, 2013.

[53] P. Aditya, et al., "Estimation of three-dimensional radar tracking using modified extended Kalman filter," in *Proc. IOP Publishing Journal of Physics: Conf. Series,* vol. 974, no. 1, 2018, doi :10.1088/1742-6596/974/1/012071.

[54] L. Ljung, "Asymptotic behavior of the extended Kalman filter as a parameter estimator for linear systems," *IEEE Trans. on Auto. Cont*., vol. 24, no. 1, pp. 36-50, 1979, doi: 10.1109/TAC.1979.1101943.

[55] X. Lin, T. Kirubarajan, Y. Bar-Shalom, and S. Maskell, "Comparison of ekf, pseudomeasurement, and particle filters for a bearing-only target tracking problem," in Signal and Data Processing of Small Targets 2002, vol. 4728. ,Aug. 2002, pp. 240–25.

[56] M. Koivisto, et.al., "High-efficiency device positioning and location-aware communications in dense 5G networks," *IEEE Comm. Mag*., vol. 55, no. 8, pp. 188-197, Aug. 2017, doi: 10.1109/MCOM.2017.1600655.

[57] O. Kanhere and T. S. Rappaport, "Outdoor sub-THz Position Location and Tracking using Field Measurements at 142 GHz," in *Proc. IEEE Int. Conf. on Commun., (ICC)*, June 2021, pp. 1–6.

[58] M. Pourhomayoun and M.L. Fowler, "Distributed computation for direct position determination emitter location," *IEEE Trans. Aero. Elect. Sys.*, vol. 50, no. 4, pp. 2878-2889, Oct. 2014, doi: 10.1109/TAES.2014.130005.

[59] GPS: The Global Positioning System. Accessed Dec 09, 2020. [Online].Available at: https://www.gps.gov/.

Jaswinder Lota (M'99–SM'09) received the B.Sc. degree from the National Defence Academy, Pune, India, the B.Eng. degree in electrical engineering from the Naval College of Engineering, Pune, the M.Eng. degree in radar and communication engineering from the Indian Institute of Technology, New Delhi, India, and the Ph.D. degree from the University of Westminster, London, U.K., in 2007. He was with the Indian Navy since 1989 in various roles in engineering for radar, EW and weapon systems. He was a Senior Technologist with Sepura Plc., Cambridge, U.K., (2006–2009) for development of TETRA-2 mobile radios. Since 2009, he has been with the University of East London, London (Senior Lecturer 2009–2014, Reader 2014-present). Since 2013, he has been a visiting academic in the Department of Electronics and Electrical Engineering, University College London, London. His research interests include wireless communications, signal processing, circuits and systems. Since 2018 he has been an Associate Editor for the IEEE TRANSACTIONS ON CIRCUITS AND SYSTEMS I: REGULAR PAPERS. He was a Guest Editor for the IEEE

TRANSACTIONS ON CIRCUITS AND SYSTEMS I: REGULAR PAPERS Special Issue 2017 on the CASS Flagship Conferences. In 2015 he was a Guest Editor for the IEEE TRANSACTIONS ON CIRCUITS AND SYSTEMS II: EXPRESS BRIEFS Special Issue on Biomedical and Bioelectronic Circuits for Enhanced Diagnosis and Therapy.

Shihao Ju (Graduate Student Member, IEEE) received the B.S. degree in communications engineering from the Harbin Institute of Technology, Harbin, China, in 2017, and the M.S. degree in electrical engineering from New York University (NYU), Brooklyn, NY, USA, in 2019, where he is currently pursuing the Ph.D. degree with the NYU WIRELESS Research Center, under the supervision of Prof. T. S. Rappaport. His research interests include millimeter-wave and Terahertz channel modeling and simulation, intelligent reflecting surface, and machine learning.

Ojas Kanhere received the B.Tech. and M.Tech. degrees in electrical engineering from IIT Bombay, Mumbai, India, in 2017. He is currently pursuing the Ph.D. degree in electrical engineering with the NYU WIRELESS Research Center, New York University (NYU) Tandon School of Engineering, Brooklyn, NY, USA, under the supervision of Prof. Rappaport. His research interests include mmWave localization and channel modeling.

Theodore S. Rappaport (S'83-M'84-SM'91- F'98) is the David Lee/Ernst Weber Professor at New York University (NYU) and holds faculty appointments in the Electrical and Computer Engineering department, the Courant Computer Science department, and the NYU Langone School of Medicine. He founded NYU WIRELESS, a multidisciplinary research center, and the wireless research centers at UT Austin (WNCG) and Virginia Tech (MPRG). His research has provided fundamental knowledge of wireless channels used to create the first Wi-Fi standard (IEEE 802.11), the first US digital TDMA and CDMA standards, the first public Wi-Fi hot spots, and more recently proved the viability of millimeter wave and sub-THz frequencies for 5G, 6G, and beyond.

Andreas Demosthenous (Fellow IEEE) received the B.Eng. degree in electrical and electronic engineering from the University of Leicester, Leicester, U.K., the M.Sc. degree in telecommunications technology from Aston University, Birmingham, U.K., and the Ph.D. degree in electronic and electrical engineering from University College London (UCL), London, U.K., in 1992, 1994, and 1998, respectively. He is currently a Professor with the Department of Electronic and Electrical Engineering, UCL, and leads the Bioelectronics Group. He has made outstanding contributions to improving safety and performance in integrated circuit design for active medical devices, such as spinal cord and brain stimulators. He has numerous collaborations for cross-disciplinary research, both within the U.K. and internationally. He has authored over 30 articles in journals and international conference proceedings, several book chapters, and holds several patents. His research interests include analog and mixed-signal integrated circuits for biomedical, sensor, and signal processing applications.

Dr. Demosthenous is a fellow of the Institution of Engineering and Technology and a Chartered Engineer. He was a co-recipient of a number of Best Paper Awards and has graduated many Ph.D. students. He was an Associate Editor from 2006 to 2007 and the Deputy Editor-in-Chief from 2014 to 2015 of the IEEE TRANSACTIONS ON CIRCUITS AND SYSTEMS II: EXPRESS BRIEFS, and an Associate Editor from 2008 to 2009 and the Editor-in-Chief from 2016 to 2019 of the IEEE TRANSACTIONS ON CIRCUITS AND SYSTEMS I: REGULAR PAPERS. He is an Associate Editor of the IEEE TRANSACTIONS ON BIOMEDICAL CIRCUITS AND SYSTEMS and serves on the International Advisory Board of Physiological Measurement. He has served on the technical committees for a number of international conferences, including the European Solid-State Circuits Conference and the International Symposium on Circuits and Systems.